Macromolecules

Article

pubs.acs.org/Macromolecules

Hydrogen Bond Interactions Mediate Hierarchical Self-Assembly of POSS-Containing Block Copolymers Blended with Phenolic Resin

Chin-Wei Chiou,[†] Yung-Chih Lin,[†] Lei Wang,[‡] Rina Maeda,[‡] Teruaki Hayakawa,*[,‡] and Shiao-Wei Kuo*[,†]

[†]Department of Materials and Optoelectronic Science, Center for Functional Polymers and Supramolecular Materials, National Sun Yat-Sen University, Kaohsiung 804, Taiwan

[‡]Department of Organic and Polymeric Materials, Tokyo Institute of Technology, 2-12-1-S8-36 O-okayama, Meguro-ku, Tokyo 152-8552, Japan

ABSTRACT: Poly(methyl methacrylate)-*b*-poly(methacryloyl polyhedral oligomeric silsesquioxane) (PMMA-*b*-PMAPOSS) block copolymers of various compositions were prepared through anionic living polymerization. We employed differential scanning calorimetry, Fourier transform infrared spectroscopy, small-angle X-ray scattering, transmission electron microscopy, and wide-angle X-ray diffraction to investigate the miscibility, specific interactions, and hierarchical self-assembly of PMMA-*b*-PMAPOSS block copolymers blended with a phenolic resin. We found that the added phenolic resin interacted preferentially with the PMMA blocks through hydrogen bonding between the OH groups of the former and the C═O groups of the PMAPOSS. In other words, the OH groups of the phenolic resin did not interact with the C═O groups of the PMAPOSS blocks, resulting in their immiscibility. Accordingly, this phenolic/PMMA-*b*-PMAPOSS blend behaved as a blend of homopolymer C and immiscible A-*b*-B diblock copolymer, where C is immiscible with B but interacts favorably with A; therefore, it displayed an order−order phase transition with increased phenolic resin content. Hierarchical self-assembly led to the formation of hexagonally packed cylindrical or lamellar nanostructures through microphase separation of the diblock copolymer segment, with POSS aggregates packing into a hexagonal lattice oriented perpendicular to the direction of the nanostructures.

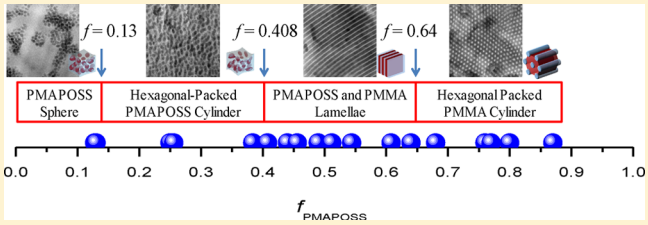

INTRODUCTION

Diblock copolymers can form a number of self-assembled nanostructures in the bulk state, including lamellae, gyroid, hexagonally packed cylinders, and body-centered cubic spheres, depending on the relative volume fraction of the blocks, total degree of polymerization, and Flory−Huggins interaction parameter.[1,2] The most frequently used diblock copolymers for nanofabrication are organic/organic block copolymers such as polystyrene-*b*-poly(4-vinylpyridine) (PS-*b*-P4VP),[3−6] polystyrene-*b*-poly(methyl methacrylate) (PS-*b*-PMMA),[7,8] and polystyrene-*b*-poly(vinylphenol) (PS-*b*-PVPh).[9−11] Blending inorganic nanoparticles (NPs) into a block copolymer provides the intriguing opportunity to engineer novel properties arising from the particular electronic, optical, and magnetic properties of individual components.[12−23] For example, Watkins et al.[18,19] reported that high loadings of NPs based on functionalized polyhedral oligomeric silsesquioxane (POSS) are possible within poly(ethylene oxide)-*b*-poly(propylene oxide)-*b*-poly(ethylene oxide) (PEO-*b*-PPO-*b*-PEO) triblock copolymers. The presence of maleamic acid or aminophenyl ligands in POSS NPs enabled selective hydrogen bonding with the PEO domains, with further addition of the additive inducing an order-to-order transition from cylindrical to spherical morphology.

In addition to the blending of inorganic NPs with organic/organic block copolymers to form block copolymer/nanoparticle (BCP/NP) composites, interest in organic/inorganic hybrid block copolymers has increased recently because the presence of inorganic NPs in block copolymers results in properties that cannot be achieved in organic/organic block copolymers. For example, a few organic/inorganic hybrid block copolymers, including polystyrene-*b*-polydimethylsiloxane (PS-*b*-PDMS)[24,25] and polystyrene-*b*-polyferrocenylsilane (PS-*b*-PFS),[26] have received attention for their use in integrated circuit processing. Several inorganic materials, including POSS units, have been incorporated within organic/inorganic block copolymers. POSS derivatives are inorganic block segments that constitute a family of molecularly precise and near-isotropic materials.[27−30] Pyun and Matyjaszewski[31,32] used atom transfer radical polymerization (ATRP) to synthesize methacryloyl POSS block copolymers (PMAPOSS) from a cyclopentyl-substituted POSS monomer and *n*-butyl acrylate. PMMA-*b*-PMAPOSS and P4VP-*b*-PMAPOSS through reversible addition−fragmentation chain transfer (RAFT) polymerization were also widely reported.[33] We have previously used a

Received: October 27, 2014
Revised: December 1, 2014
Published: December 11, 2014

   dx.doi.org/10.1021/ma502180c | *Macromolecules* 2014, 47, 8709−8721

Scheme 1. Synthesis of PMMA-*b*-PMAPOSS Diblock Copolymers through Living Anionic Polymerization

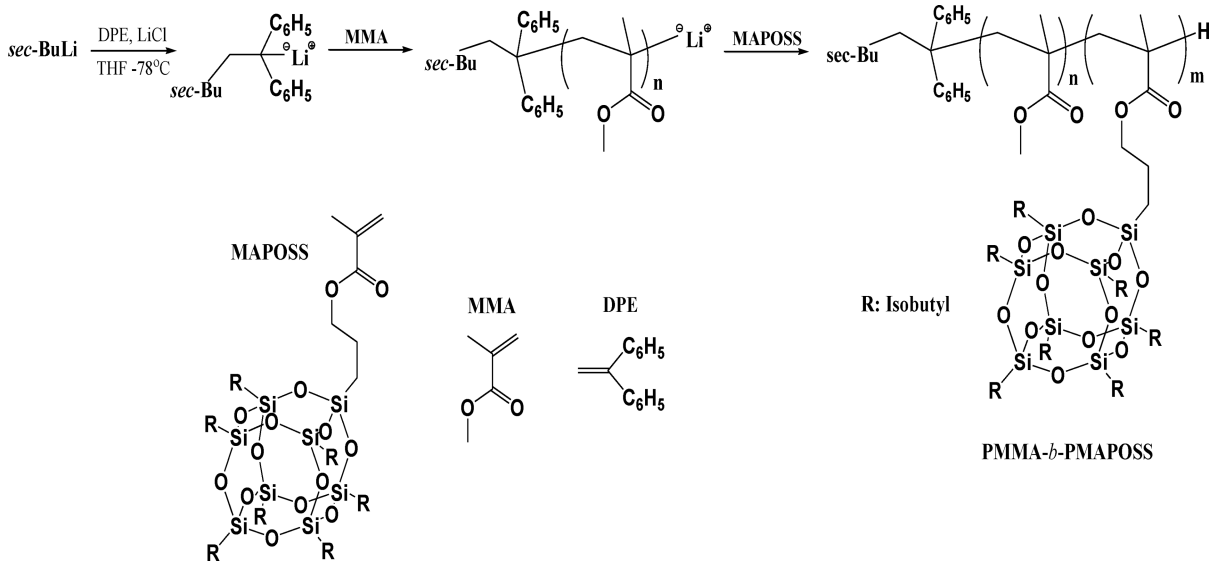

combination of ATRP, ring-opening polymerization, and click chemistry to synthesize polystyrene-*b*-poly(γ-propargyl-L-glutamate-*g*-polyhedral oligomeric silsesquioxane) [PS-*b*-(PPLG-*g*-POSS)] derivatives as new organic/inorganic macromolecular self-assembling building blocks.[34] Hirai et al.[35] prepared PMMA-*b*-PMAPOSS through anionic living polymerization and found that these block copolymers self-assembled into various structures, including spherical, cylindrical, and lamellar morphologies.

In the syntheses of these diblock copolymers, it can be relatively difficult to control the volume fraction of each block copolymer because it is necessary to synthesize different volume fractions of each block copolymer segments. The formation of a BCP/NP hybrid block copolymer is conceptually similar to the blending of a homopolymer C with an organic/inorganic (A-*b*-B) diblock copolymer, where C can interact noncovalently (e.g., through hydrogen bonds) and be miscible with the organic (A) block segment[36−45] but immiscible with the inorganic (B) one, allowing control of the volume fraction through simple blending. Hence, in this study, we prepared a series of organic/inorganic diblock copolymers (PMMA-*b*-PMAPOSS) through anionic living polymerization (Scheme 1), which were then blended with a phenolic resin, an organic homopolymer capable of hydrogen bond interactions. Phenolic/PMMA systems are miscible blends that we have studied extensively and found to have an interassociation equilibrium constant (K_A) of 20, which was determined through a least-squares fitting procedure based on the fraction of hydrogen-bonded C═O groups measured experimentally.[46,47] In contrast, phenolic/PMA−POSS blends are immiscible because of strong intramolecular screening effect ($\gamma = 1$), where the intramolecular screening effect defined as the fraction of same-chain contacts originating from polymer chain self-bending, primarily through local but also through long-range, connectivity effects and thus the presence of POSS nanoparticles on the side chains of PMMA inhibits the interaction of phenolic OH groups with the C═O groups of PMAPOSS.[48] To the best of our knowledge, this paper describes the first example of an organic/inorganic diblock copolymer in which volume fractions can be controlled through blending with an organic homopolymer capable of hydrogen bond interactions. Differential scanning calorimetry (DSC), wide-angle X-ray diffraction (WAXD), transmission electron microscopy (TEM), small-angle X-ray scattering (SAXS), and Fourier transform infrared (FTIR) spectroscopy were used to characterize the self-assembly and specific interactions of these phenolic/PMMA-*b*-PMAPOSS hybrids.

EXPERIMENTAL SECTION

Materials. Methyl methacrylate (MMA, 99%, SHOWA) was distilled from finely ground CaH_2 prior to use. Hepta-(isobutylpentacyclooctasiloxan-1-yl)propyl methacrylate (MAPOSS, Hybrid Plastics) was dissolved in tetrahydrofuran (THF) and subsequently precipitated with MeCN. The purified MAPOSS monomer was then recrystallized from MeOH and dried in a vacuum oven at 60 °C overnight. THF was freshly distilled over Na/benzophenone (deep purple) after heating under reflux for 2 h under N_2. 1,1-Diphenylethylene (DPE) was distilled from *n*-BuLi. LiCl was dried overnight at 160 °C in a vacuum oven. *sec*-BuLi (1.3 M in cyclohexane, Chemetall) was used as received. The phenolic resin was synthesized through a H_2SO_4-catalyzed condensation reaction, producing an average molecular weight (M_n) of 500, PDI = 2.40, using the procedure described previously.[49]

PMMA-*b*-PMAPOSS Block Copolymers through Living Anionic Polymerization. A glass reactor containing dry LiCl (25 mg, 0.61 mmol) was charged with THF (40 mL) and subsequently cooled to −78 °C under Ar. After 5 min, *sec*-BuLi was added until the color became light yellow. The reactor was removed from the cooling bath and warmed to room temperature until the solution became colorless. The reactor was again cooled to −78 °C after which *sec*-BuLi (0.035 mL, 0.046 mmol) was added. After 5 min, DPE (0.04 mL, 0.23 mmol) was added, resulting in a deep red color. After 30 min, MMA (0.6 mL, 5.6 mmol) was added via cannula to the polymerization reactor with vigorous stirring. The deep red color disappeared to give a light yellow solution. After 30 min, a solution of MAPOSS (2.00 g, 2.1 mmol) in THF (6.0 mL) was added to the polymerization reactor via cannula with vigorous stirring. The deep red color disappeared to give a colorless solution. After 9 h at −78 °C, an excess of MeOH was added to terminate the reaction. The polymer was then precipitated with MeOH and dried overnight at 60 °C in a vacuum oven. A yield of 1.9 g (74%) was obtained.

Blend Preparation. Blends of phenolic/PMMA-*b*-PMAPOSS with various compositions were prepared through solution casting. A THF solution containing 5 wt % of the polymer mixture was stirred for 6−8 h, and then, the solvent was evaporated slowly at 50 °C for 1 day. The

dx.doi.org/10.1021/ma502180c | Macromolecules 2014, 47, 8709−8721

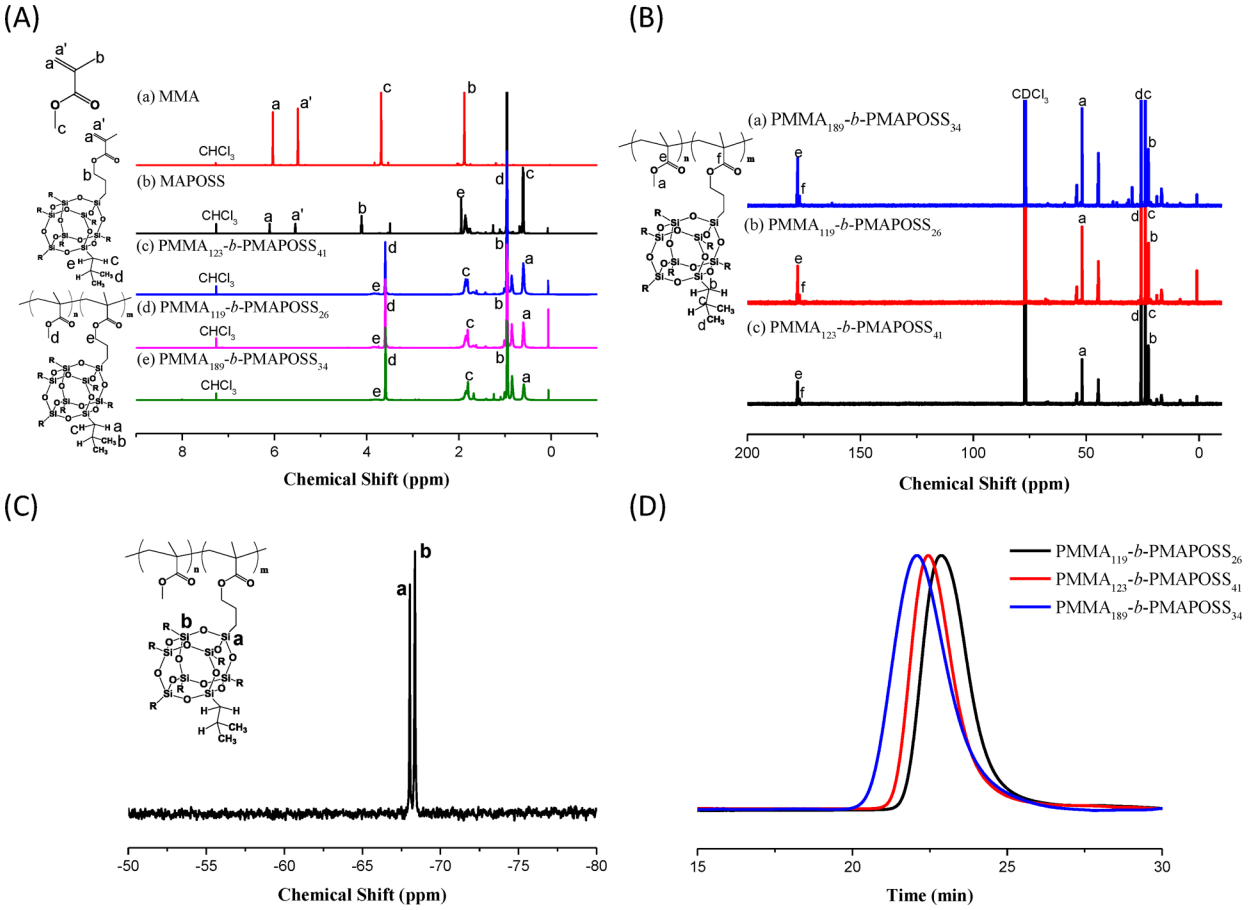

Figure 1. Characterization of PMMA-*b*-PMAPOSS diblock copolymers: (A) ^{1}H, (B) ^{13}C, and (C) ^{29}Si NMR spectra; (D) MALLS analysis.

blend film was then dried at 80 °C for 2 days to ensure total removal of residual solvent.

Characterization. ^{1}H, ^{13}C, and ^{29}Si NMR spectra were recorded at room temperature using a Bruker AM 500 (500 MHz) spectrometer, with the residual proton resonance of the deuterated solvent as the internal standard. Molecular weights and molecular weight distributions were determined through gel permeation chromatography (GPC) using a Waters 510 high-performance liquid chromatograph equipped with a Waters 410 differential refractometer and three Ultrastyragel columns (100, 500, and 103 Å) connected in series, with THF as the eluent (flow rate: 1.0 mL/min). A multiple-angle laser light scattering (MALLS) detector (miniDAWN Model, Wyatt Technology) was equipped with a 20 mW semiconductor laser, enabling determination of the "true" molecular weight. For the molecular weight calculation, the d*n*/d*c* (specific refractive index increment) of the synthesized polymer at the same wavelength of light as that of MALLS was measured using a Wyatt Optilab DSP interferometric refractometer. DSC was performed using a TA-Q20 instrument operated at a scan rate of 20 °C/min over the temperature range 0−250 °C under a N_2 atmosphere. The FTIR spectra of the polymer films, sufficiently thin to obey the Beer−Lambert law, were recorded using the conventional KBr disk method and a Bruker Tensor 27 FTIR spectrophotometer; 32 scans were collected at a spectral resolution of 1 cm^{-1}. Because polymers containing OH groups are hygroscopic, pure N_2 gas was used to purge optical box of the spectrometer to ensure that sample films are dry. The FTIR spectra of the samples were recorded at elevated temperatures using a cell mounted within the temperature-controlled compartment of the spectrometer. The WAXD and SAXS data were collected using the BL17A1 wiggler beamline of the National Synchrotron Radiation Research Center (NSRRC), Taiwan. For WAXD, a triangular bent Si (111) single crystal was employed to obtain a monochromated beam with a wavelength of 1.33 Å; all the temperature-resolved SAXS measurements were performed at several temperatures on a hot stage under a dry N_2 atmosphere. The samples were sealed between two Kapton windows (thickness: 12 μm). An X-ray beam having a diameter of 0.5 mm and wavelength of 1.12 Å was used for the SAXS measurements. TEM images were recorded using a JEOL JEM-2100 transmission electron microscope operated at an accelerating voltage of 200 kV. Ultrathin sections of the TEM samples (thickness: ∼70 nm) were prepared using the Leica Ultracut UCT Microtome equipped with a diamond knife.

RESULTS AND DISCUSSION

Synthesis of PMMA-*b*-PMAPOSS. In this study, the method used to prepare the PMMA-*b*-PMAPOSS diblock copolymers was similar to that reported by Hirai et al.,[35] involving living anionic polymerization initiated by *sec*-BuLi in the presence of excess LiCl and DPE at −78 °C (Scheme 1). Figure 1 presents the ^{1}H, ^{13}C, and ^{29}Si NMR spectra and MALLS data for these diblock copolymers. The signals for the olefinic bonds of the MMA and MAPOSS monomers at 6.02 and 5.47 ppm, respectively, disappeared from the ^{1}H NMR spectra of PMMA-*b*-PMAPOSS (Figure 1a). The spectrum of the latter features signals for the $SiCH_2$ (g) units of the POSS cage, OCH_2 (f) units of the side chains, and OCH_3 (a) units of PMMA at 0.59, 3.83, and 3.59 ppm, respectively, which indicates the successful synthesis of PMMA-*b*-PMAPOSS. The ^{13}C NMR spectrum (Figure 1b) features corresponding signals for the carbon nuclei of PMAPOSS at 22.41, 54.12, and 51.81 ppm. The ^{29}Si NMR spectrum (Figure 1c) presents two sharp signals at −68.4 and −68.0 ppm corresponding to the Si nuclei of the POSS units. The MALLS analysis in Figure 1d indicates

dx.doi.org/10.1021/ma502180c | *Macromolecules* 2014, 47, 8709−8721

Table 1. Molecular Weight (M_n), Composition, Polydispersity Index (PDI), and Morphology of PMMA-*b*-PMAPOSS Block Copolymers Used in This Study

PMMA-*b*-PMAPOSS[a]	M_n (GPC)[b]	M_n (MALLS)[c]	PMMA[d] (mol %)	PMMA[d] (wt %)	PMMA[e] (vol %)	PDI[c]	morphology[f]
$PMMA_{189}$-*b*-$PMAPOSS_{34}$	50 500	44 300	85	37	36	1.08	lamellae
$PMMA_{119}$-*b*-$PMAPOSS_{26}$	39 700	29 200	82	33	32	1.01	PMMA cylinder
$PMMA_{123}$-*b*-$PMAPOSS_{41}$	50 800	40 100	75	24	24	1.01	PMMA cylinder

[a]Numbers denote final compositions determined through gel permeation chromatography (GPC, calibrated against polystyrene linear standards) and integrated ^{1}H NMR spectra. [b]Measured using GPC. [c]Measured using multiple-angle laser light scattering (MALLS). [d]Determined from ^{1}H NMR spectra. [e]Determined from density gradient column, integrated ^{1}H NMR spectra, and GPC. [f]Observed using TEM.

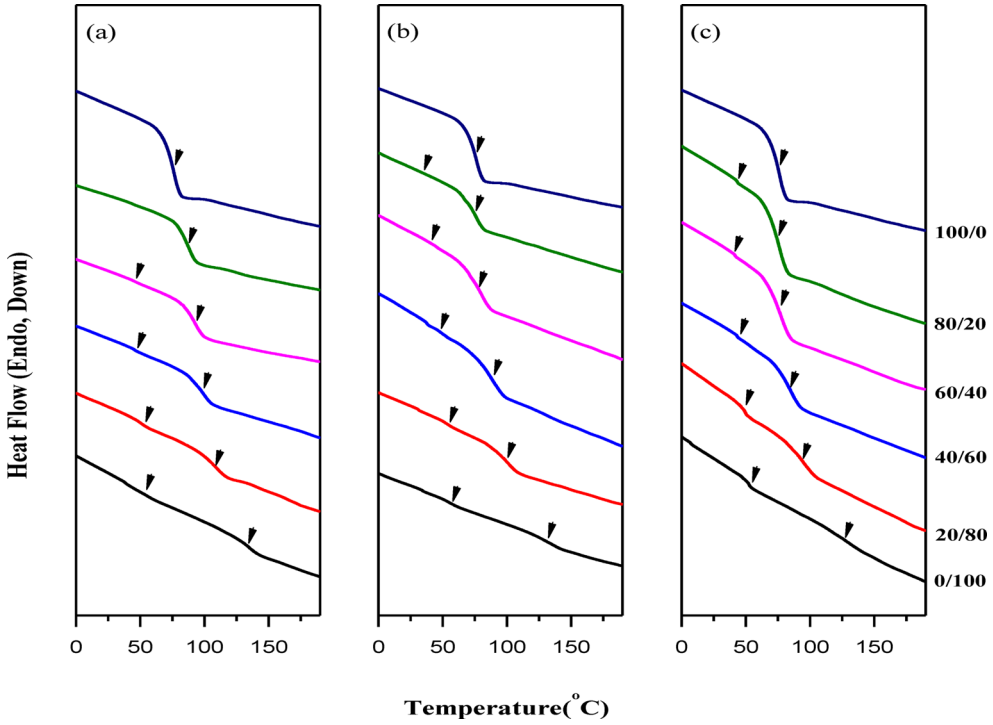

Figure 2. DSC thermograms of (a) phenolic/$PMMA_{189}$-*b*-$PMAPOSS_{34}$, (b) phenolic/$PMMA_{119}$-*b*-$PMAPOSS_{26}$, and (c) phenolic/$PMMA_{123}$-*b*-$PMAPOSS_{41}$ blends at various phenolic weight ratios.

that the number-average molecular weights (M_n) of the PMMA-*b*-PMAPOSS samples are 44 300, 40 100, and 29 200 g/mol, with polydispersity indices (PDIs) of 1.08, 1.01, and 1.01, respectively. Thus, the ^{1}H, ^{13}C, and ^{29}Si NMR spectra and MALS analysis collectively confirmed the successful synthesis of the PMMA-*b*-PMAPOSS diblock copolymers, and the specific compositions are summarized in Table 1.

DSC Analyses. Figure 2 displays the conventional second-run DSC thermograms of the PMMA-*b*-PMAPOSS diblock copolymers blended with the phenolic resin at various weight ratios. The pure diblock copolymers displayed two glass transition temperatures, representing the two different types of segments present in the polymer chains. The lower T_g occurred near 50 °C, corresponding to large PMAPOSS segments. On the other hand, the higher T_g (~135 °C) was assigned to PMMA segments. The T_g of the pure phenolic resin was approximately 76 °C. All blends displayed two distinct values of T_g, suggesting that microphase separation occurred in these phenolic/PMMA-*b*-PMAPOSS blends. The T_g of the PMMA block decreased significantly, whereas that of the PMAPOSS block remained almost unchanged, upon increasing the phenolic resin content. Therefore, it was presumed that the added phenolic resin interacted preferentially with the PMMA blocks through hydrogen bonding between the OH groups of the former and the C═O groups of the latter. In other words, the OH groups of the phenolic resin did not interact with the C═O groups of the PMAPOSS blocks, resulting in their immiscibility. This can be attributed to a strong screening effect from the tethered POSS side chains, as discussed in previous studies.[47,48] We propose that the intramolecular screening effect (γ) should be very close to 1 for all PMAPOSS blend systems. This denotes that POSS nanoparticles with hydrogen bond donors are present in the side chains of PMMA because the OH groups of, for example, the phenolic resin cannot interact with the C═O groups of PMAPOSS.

Although the phenolic resin was miscible with PMMA block segments, the behavior of the glass transition temperature of the phenolic/PMMA miscible phase at varying weight fractions of the PMAPOSS segments was examined as shown in Figure 3. A dependence between these two parameters was observed. The relationship between the glass transition temperature and the composition of a miscible blend generally follows the Kwei equation[50]

$$T_g = \frac{W_1 T_{g1} + kW_2 T_{g2}}{W_1 + kW_2} + qW_1W_2 \quad (1)$$

dx.doi.org/10.1021/ma502180c | Macromolecules 2014, 47, 8709−8721

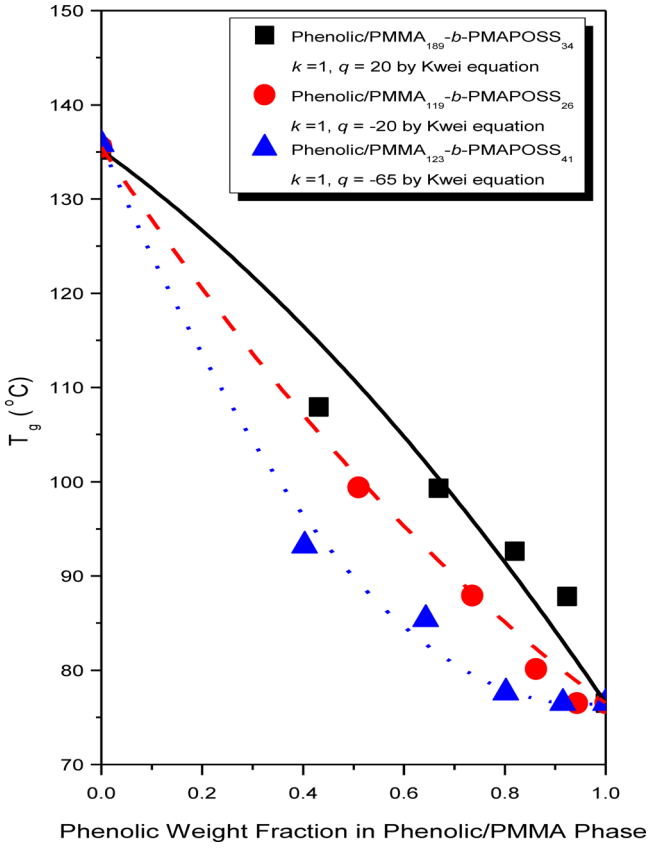

Figure 3. Glass transition temperature (T_g)–composition curves of phenolic/PMMA-*b*-PMAPOSS blends based on the Kwei equation.

where W_1 and W_2 are the weight fractions of the components, T_{g1} and T_{g2} represent the corresponding glass transition temperatures, and k and q are the fitting constants, with the latter denoting the strength of specific interactions in the blend. As displayed in Figure 3, the k and q values obtained using a nonlinear least-squares "best fit" approach are respectively 1 and 20 for phenolic/$PMMA_{189}$-*b*-$PMAPOSS_{34}$, 1 and −20 for phenolic/$PMMA_{119}$-*b*-$PMAPOSS_{26}$, and 1 and −65 for phenolic/$PMMA_{123}$-*b*-$PMAPOSS_{41}$.

FTIR Spectroscopic Analyses. Infrared spectroscopy can provide both qualitative and quantitative information on specific interactions between polymers. Figure 4 presents the FTIR spectra of selected phenolic/$PMMA_{189}$-*b*-$PMAPOSS_{34}$ blends recorded at room temperature. The spectrum of the pure phenolic resin (Figure 4a) features two distinct bands in the OH stretching region: a very broad band centered at 3360 cm^{-1} representing the wide distribution of hydrogen-bonded OH groups and a sharp band near 3525 cm^{-1} for the free OH groups. In general, the intensity of the signal for the latter decreased upon increasing the $PMMA_{189}$-*b*-$PMAPOSS_{34}$ content, as would be expected. On the other hand, the broad signal for hydrogen-bonded OH groups shifted to a higher frequency (3430 cm^{-1}) upon increasing the $PMMA_{189}$-*b*-$PMAPOSS_{34}$ content to 80 wt %. These changes arose from the transformation from intramolecular OH···OH to intermolecular OH···O=C bonds.[51−53] Similarly, C=O stretching vibrations were sensitive to hydrogen bond formation.

Figure 4b displays the C=O stretching region of the FTIR spectra of the phenolic/$PMMA_{189}$-*b*-$PMAPOSS_{34}$ blends at room temperature. The C=O stretching frequencies were split into two bands: one at 1730 cm^{-1} corresponding to the free C=O groups in PMMA-*b*-PMAPOSS and the other at 1706 cm^{-1} representing the hydrogen-bonded ones. Figure 5 displays the results of least-squares curve fitting for the C=O stretching region using two Gaussian bands. Through quantitative measurement of the absorptivity ratio (a_R) of these two bands, the fraction of hydrogen-bonded C=O units can be determined by using $a_R = a_{HB}/a_F = 1.5$.[51−53] Table 2 summarizes the spectroscopic and calculated parameters for the C=O groups. The fraction of hydrogen-bonded C=O groups in PMMA-*b*-PMAPOSS increased upon increasing the phenolic content. Free C=O groups were found in both

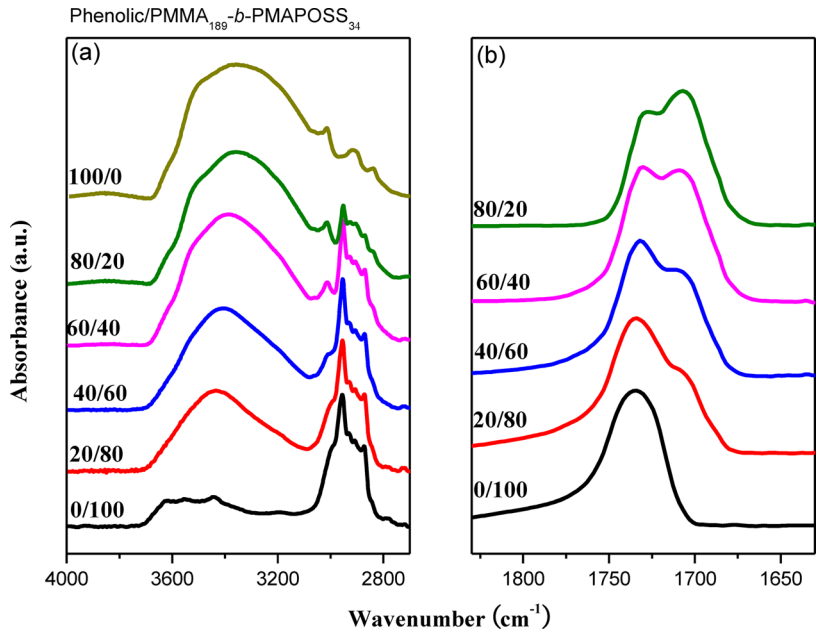

Figure 4. FTIR spectra of phenolic/$PMMA_{189}$-*b*-$PMAPOSS_{34}$ blends at various phenolic compositions recorded at room temperature: (a) OH and (b) C=O stretching.

dx.doi.org/10.1021/ma502180c | Macromolecules 2014, 47, 8709−8721

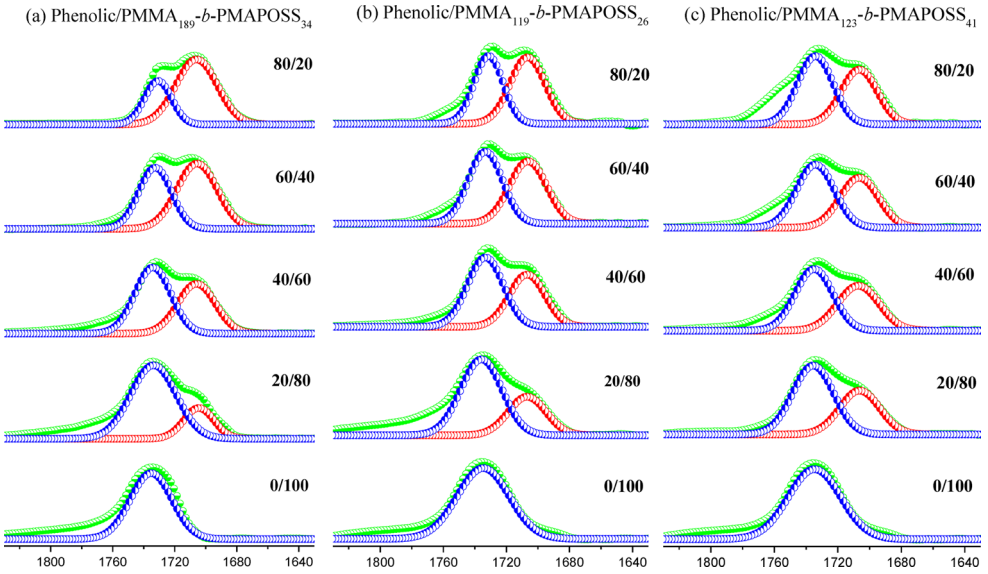

Figure 5. Deconstructed C═O stretching bands of (a) phenolic/$PMMA_{189}$-*b*-$PMAPOSS_{34}$, (b) phenolic/$PMMA_{119}$-*b*-$PMAPOSS_{26}$, and (c) phenolic/$PMMA_{123}$-*b*-$PMAPOSS_{41}$ blends at various phenolic compositions. The green curve represents the original band while the blue and red curves represent respectively the free and hydrogen-bonded C═O groups.

Table 2. Fraction of Hydrogen-Bonded C═O Groups (f_b) in Phenolic/PMMA-*b*-PMAPOSS Blends from Curve-Fitting of FTIR Spectroscopic Data

	free C═O		hydrogen-bonded C═O		
	ν_f (cm^{-1})	A_f (%)	ν_b (cm^{-1})	A_b (%)	f_b
phenolic/$PMMA_{189}$-*b*-$PMAPOSS_{34}$					
0/100	1736	100		0	0
20/80	1734	78.3	1705	21.7	15.6
40/60	1734	56.0	1705	44.0	34.4
60/40	1732	43.2	1705	56.8	46.7
80/20	1731	30.4	1705	69.6	60.4
phenolic/$PMMA_{119}$-*b*-$PMAPOSS_{26}$					
0/100	1735	100		0	0
20/80	1735	68.3	1706	31.7	23.6
40/60	1733	56.0	1706	44.0	34.4
60/40	1733	51.4	1706	48.6	38.7
80/20	1731	45.7	1706	54.3	44.2
phenolic/$PMMA_{123}$-*b*-$PMAPOSS_{41}$					
0/100	1735	100		0	0
20/80	1735	61.6	1706	38.4	29.4
40/60	1735	55.4	1706	44.6	34.9
60/40	1734	55.3	1706	44.7	35.0
80/20	1734	54.9	1706	45.1	35.4

PMMA and PMAPOSS block segments; in contrast, the hydrogen-bonded C═O groups were only due to the interaction of PMMA block segments with the phenolic resin. In a previous study,[48] we did not observe any hydrogen-bonded C═O groups in PMAPOSS after blending with a phenolic resin, which was rationalized in terms of the screening effect. Therefore, digital subtraction of the pure PMAPOSS peak at 1730 cm^{-1} was performed based on its mole fraction in the diblock copolymers[54] (Figure 6), and the corrected fractions of hydrogen-bonded C═O groups in the PMMA block segment are summarized in Figure 7. Although the fraction generally increased upon increasing the phenolic content, the trends were quite different in the three PMMA-*b*-PMAPOSS block copolymers. The fraction of hydrogen-bonded C═O groups in the PMMA block segment in the phenolic/$PMMA_{189}$-*b*-$PMAPOSS_{34}$ blend was larger than that in the binary homopolymer phenolic/PMMA blend at all compositions. For the phenolic/$PMMA_{119}$-*b*-$PMAPOSS_{26}$ and phenolic/$PMMA_{123}$-*b*-$PMAPOSS_{41}$ blends, the fraction was larger than those in phenolic/PMMA blends when the phenolic content was less than 60 wt % and smaller when the phenolic content was 80 wt %. As a result, increasing the weight fraction of PMAPOSS in the block copolymer at a relatively high phenolic content (80 wt %) decreased the fraction of intermolecular hydrogen bonds between the C═O groups of the PMMA block segment and the OH groups of the phenolic resin, while at a relatively low phenolic content (20 wt %), the highest fraction of hydrogen-bonded C═O groups was obtained. Thus, the fraction of hydrogen-bonded C═O groups in these phenolic/PMMA-*b*-PMAPOSS blends was strongly dependent on the phenolic content and weight fraction of the PMAPOSS segment in the block copolymer.

Self-Assembly of Phenolic/PMMA-*b*-PMAPOSS Blends. Figure 8 presents the SAXS profiles of the phenolic/PMMA-*b*-PMAPOSS blends recorded at room temperature to confirm the presence of microphase-separated morphologies. SAXS analysis revealed a lamellar microdomain structure for the pure $PMMA_{189}$-*b*-$PMAPOSS_{34}$ block copolymer (Figure 8a), consistent with the TEM image in Figure 9a. The scattering maxima at relative positions of 1:2:3:4 correspond to a domain spacing of 46.8 nm (q = 0.134 nm^{-1}). The lamellar microdomain structure is associated with a larger-scale copolymer domain structure arising from the microphase separation of the PMMA and PMAPOSS blocks. The addition of 20 wt % phenolic resin to the $PMMA_{189}$-*b*-$PMAPOSS_{34}$ block copolymer resulted in peak broadening with scattering maxima at relative positions of 1:2:3:4, suggesting the short-range order of a lamellar morphology as confirmed by the TEM image in Figure 9b. In addition, the first-order scattering

dx.doi.org/10.1021/ma502180c | *Macromolecules* 2014, 47, 8709−8721

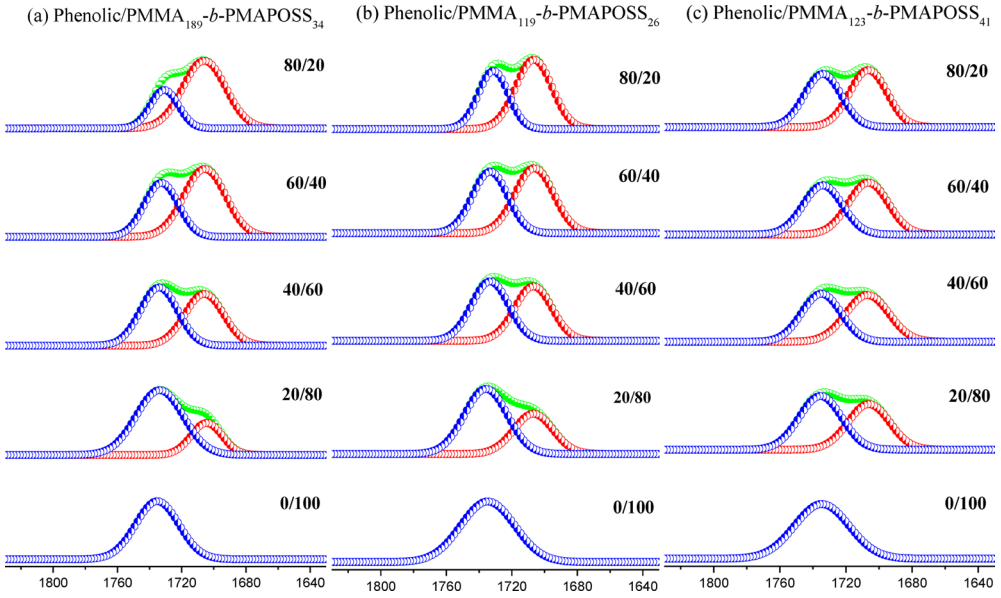

Figure 6. Deconstructed C═O stretching bands of (a) phenolic/$PMMA_{189}$-*b*-$PMAPOSS_{34}$, (b) phenolic/$PMMA_{119}$-*b*-$PMAPOSS_{26}$, and (c) phenolic/$PMMA_{123}$-*b*-$PMAPOSS_{41}$ blends at various phenolic compositions after digital subtraction according to PMAPOSS molar ratios. The green curve represents the original band while the blue and red curves represent respectively the free and hydrogen-bonded C═O groups.

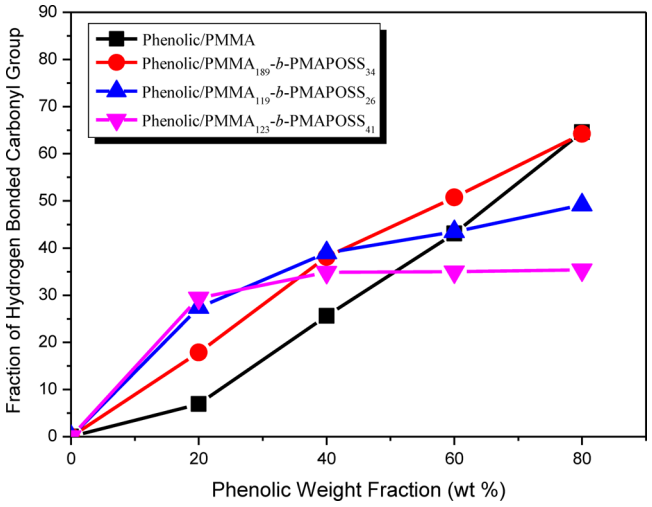

Figure 7. Fraction of hydrogen-bonded C═O groups in PMMA at various phenolic/PMMA and phenolic/PMMA-*b*-PMAPOSS blends determined from FTIR spectra.

position shifted to the lower q region upon increasing the phenolic content up to 20 wt % (q_{max} = 0.09 nm^{-1}, d-spacing = 69.7 nm), indicating an increase in the interlamellar spacing. Upon increasing the phenolic content to 40 and 60 wt %, the d-spacing decreased to 52.6 nm (q_{max} = 0.119 nm^{-1}) and 40.5 nm (q_{max} = 0.155 nm^{-1}), respectively, accompanied by broad shoulder peaks with $\sqrt{3}$ and 2. This corresponds to the short-range order of a cylindrical structure as confirmed in the TEM images in Figures 9c and 9d, respectively. Further increase of the phenolic content to 80 wt % resulted in a d-spacing of 50.2 nm (q_{max} = 0.155 nm^{-1}) and two shoulder peaks with $\sqrt{3}$ and $\sqrt{7}$, corresponding to a PMAPOSS spherical micelle structure. When the volume fraction of the PMAPOSS block decreased significantly to approximately 12.8%, individual PMAPOSS spheres having a diameter of approximately 30−40 nm were observed (Figure 9e). A transition occurred from lamellar to cylindrical and then to spherical micelle structures; this additive-induced morphological transition was driven by both increase in the effective interaction parameter and change in the overall volume fraction of the two microphase-separated domains. Nevertheless, because of the tethered POSS nanoparticles on the side chains, the PMAPOSS blocks formed a randomly oriented helixlike structure to relieve the steric crowding of the POSS units in the absence of thermal annealing.[35] As a result, it was difficult to form the long-range order of hexagonally packed PMAPOSS cylindrical and spherical structures. In the TEM images in Figure 9, which were obtained without any staining, the dark regions were attributed to the POSS-rich layers because the Si atoms of PMAPOSS provided a higher mass contrast relative to the organic domains. In the minor domain, the bright regions correspond to the PMMA or phenolic/PMMA miscible phase.

SAXS analyses revealed the long-range order of a hexagonally packed PMMA cylindrical structure for the pure $PMMA_{119}$-*b*-$PMAPOSS_{26}$ block copolymer (Figure 8b), consistent with the TEM image in Figure 9f. This is based on the scattering maxima appearing at relative positions of $1:\sqrt{3}:\sqrt{4}:\sqrt{7}:\sqrt{9}:\sqrt{12}$, corresponding to a domain spacing of 33.4 nm (q = 0.188 nm^{-1}). Interestingly, the addition of 20 and 40 wt % phenolic resin to the $PMMA_{119}$-*b*-$PMAPOSS_{26}$ block copolymer resulted in an order−order transition from the cylindrical to lamellar structure, with d-spacings of 45.5 (q_{max} = 0.138 nm^{-1}) and 52.3 nm (q_{max} = 0.12 nm^{-1}), respectively, as determined from the scattering maxima appearing at relative positions of 1:2:3:4:5:6:7:8. The TEM images in Figures 9g and 9h confirmed the high long-range order of these lamellar structures. Similarly, the first-order scattering position shifted to the lower q region upon increasing the phenolic content to 20 and 40 wt %, indicating an increase in the interlamellar spacing. It was also found that even-order peaks were suppressed at 20 wt % phenolic content owing to the structure factors of the lamellae, implying that the volume fractions of the phenolic/PMMA and PMAPOSS phases were similar ($f^{v}_{PMAPOSS}$ = 0.54).[55] Evidently, an order−order transition from cylindrical to lamellar structure could be induced through the simple

dx.doi.org/10.1021/ma502180c | *Macromolecules* 2014, 47, 8709−8721

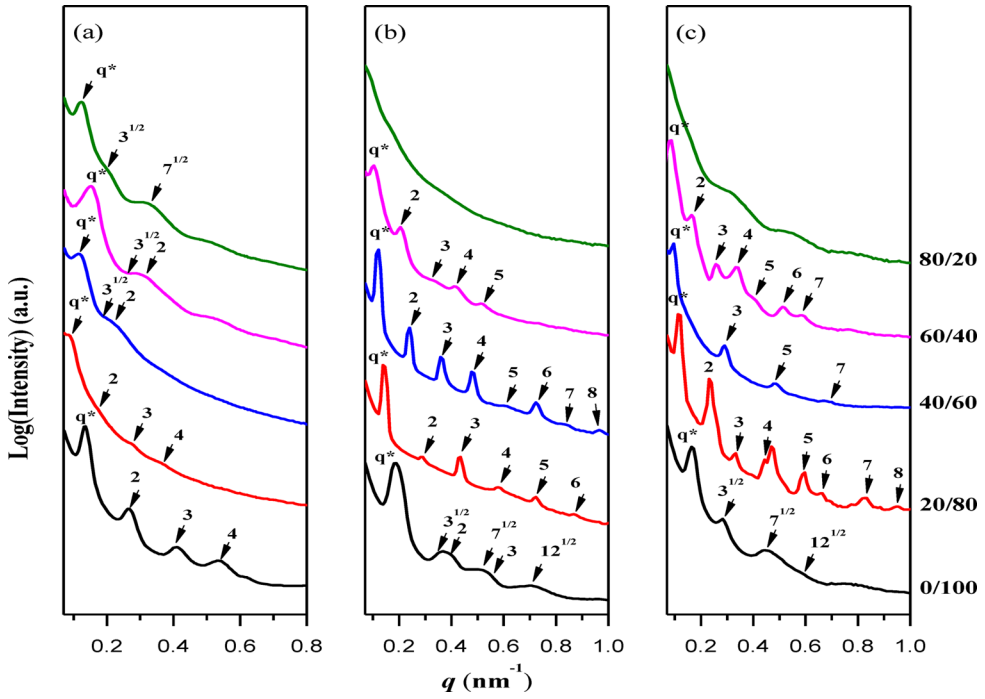

Figure 8. SAXS patterns of (a) phenolic/$PMMA_{189}$-*b*-$PMAPOSS_{34}$, (b) phenolic/$PMMA_{119}$-*b*-$PMAPOSS_{26}$, and (c) phenolic/$PMMA_{123}$-*b*-$PMAPOSS_{41}$ blends at various phenolic compositions recorded at room temperature.

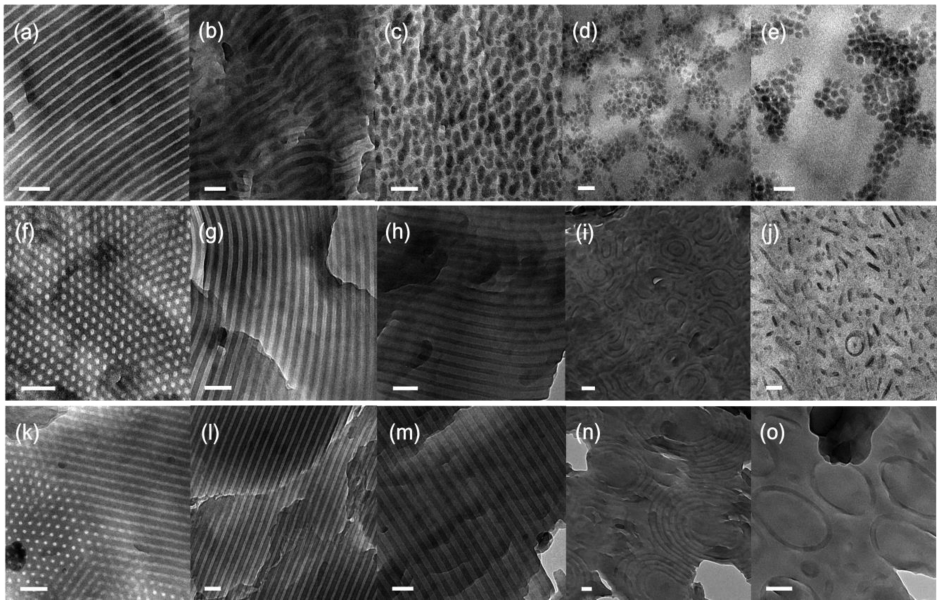

Figure 9. TEM images of phenolic/$PMMA_{189}$-*b*-$PMAPOSS_{34}$ = (a) 0/100, (b) 20/80, (c) 40/60, (d) 60/40, (e) 80/20; phenolic/$PMMA_{119}$-*b*-$PMAPOSS_{26}$ = (f) 0/100, (g) 20/80, (h) 40/60, (i) 60/40, (j) 80/20; and phenolic/$PMMA_{123}$-*b*-$PMAPOSS_{41}$ = (k) 0/100, (l) 20/80, (m) 40/60, (n) 60/40, (o) 80/20 (scale bar = 100 nm).

blending of the phenolic resin into the PMMA-*b*-PMAPOSS block copolymer mediated by hydrogen bond interactions. Upon increasing the phenolic content to 60 wt %, the *d*-spacing increased to 62.8 nm (q_{max} = 0.10 nm^{-1}) accompanied by broad peaks at a ratio of 1:2:3:4:5. This corresponds to the short-range order of a lamellar structure, as confirmed by the TEM image in Figure 9i. Further increase of the phenolic content to 80 wt % caused only broad peaks to appear in the SAXS pattern, indicating a near disordered and short−long ordered micelle morphology, as revealed in the TEM image in Figure 9j.

Figure 8c presents the SAXS profiles of the $PMMA_{123}$-*b*-$PMAPOSS_{41}$ block copolymer blended with the phenolic resin. The pure $PMMA_{123}$-*b*-$PMAPOSS_{41}$ block copolymer also displayed the long-range order of a hexagonally packed PMMA cylindrical structure, consistent with the TEM image in Figure 9k. This is based on the scattering maxima appearing at relative positions of $1:\sqrt{3}:\sqrt{7}:\sqrt{12}$, corresponding to a domain spacing of 38.5 nm (q = 0.163 nm^{-1}). Similar to the phenolic/$PMMA_{119}$-*b*-$PMAPOSS_{26}$ blend, the addition of 20 and 40 wt % phenolic resin into the $PMMA_{123}$-*b*-$PMAPOSS_{41}$ block copolymer caused an order−order transition from

dx.doi.org/10.1021/ma502180c | *Macromolecules* 2014, 47, 8709−8721

cylindrical to lamellar structures, consistent with the TEM images in Figures 9l and 9m, respectively. The corresponding *d*-spacings are 54.6 nm (q_{max} = 0.115 nm^{-1}) and 66.1 nm (q_{max} = 0.095 nm^{-1}), respectively, as determined from the scattering maxima appearing at relative positions of 1:2:3:4:5:6:7:8. Compared with the phenolic/$PMMA_{119}$-*b*-$PMAPOSS_{26}$ blends, the phenolic/$PMMA_{123}$-*b*-$PMAPOSS_{41}$ blends displayed large *d*-spacings because of the higher molecular weight of the block copolymer in this blend. In addition, it was also observed that even-order peaks disappeared at 40 wt % phenolic content owing to the structure factors of the lamellae, implying that the volume fractions of the phenolic/PMMA and PMAPOSS phases were similar ($f^{v}_{PMAPOSS}$ = 0.46). Upon increasing the phenolic content to 60 wt %, the *d*-spacing increased to 73.8 nm (q_{max} = 0.085 nm^{-1}) accompanied by broad peaks at a ratio of 1:2:3:4:5:6:7. This corresponds to a lamellar structure, as confirmed by the TEM image in Figure 9n. Moreover, the image shows that the packing of these lamellar microdomains resulted in onionlike structures. Similar structures have been observed with the binary mixtures of a poly(styrene-*b*-isoprene) block copolymer and polystyrene (PS) homopolymer when the PS content was greater than 60 wt % in the blend.[56,57] Further increasing the phenolic content to 80 wt % resulted in only broad peaks appearing in the SAXS pattern, indicating a near disordered and short−long ordered morphology (macrophase separation), as revealed in the TEM image in Figure 9k. Macrophase/microphase separation with a large cycle ring was observed at this composition, in which the PMAPOSS was dispersed in a continuous phenolic/PMMA matrix.

Scheme 2 depicts the self-assembled structures of the phenolic/PMMA-*b*-PMAPOSS blends based on the TEM images in Figure 9. The well-defined long-range order of the lamellar structure of pure $PMMA_{189}$-*b*-$PMAPOSS_{34}$ block copolymer (64 vol % PMAPOSS) and cylindrical structures of pure $PMMA_{119}$-*b*-$PMAPOSS_{26}$ (68 vol % PMAPOSS) and $PMMA_{123}$-*b*-$PMAPOSS_{41}$ (76 vol % PMAPOSS) were observed. After blending 20 wt % phenolic resin into these three block copolymers, the resulting blends displayed lamellar structures, with corresponding PMAPOSS volume fractions of 51.2, 54.4, and 60.8%, respectively. In addition, the fraction of hydrogen-bonded C═O groups in the PMMA block segments at 20 wt % phenolic resin was larger than those in phenolic/PMMA blends, as revealed in Figure 7. Painter et al.[58] reported

Scheme 2. Self-Assembled Structures of Phenolic/PMMA-*b*-PMAPOSS Blends Based on TEM Image Analyses

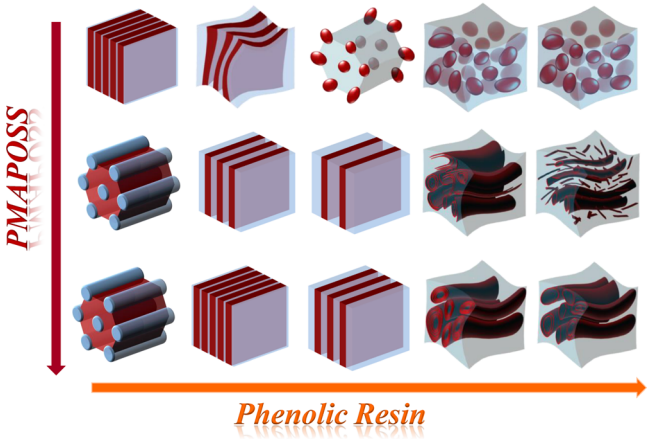

that the K_A for poly(vinylphenol) (PVPh)/PMMA blends is 37.5, whereas the K_A for a corresponding model compound mixture, ethyl phenol/ethyl isobutyrate, is 172. The significant decrease in the K_A of PVPh/PMMA blends was attributed to the effects of intramolecular screening and functional group accessibility caused by the chain connectivity.[59−63] Intramolecular screening occurs when the polymer chain bends back on itself; accordingly, the degree of interassociation hydrogen bonding in the polymer blend would be lower than in the model compound. On the other hand, the effect of functional group accessibility can be attributed to steric crowding and shielding; that is, the spacing between the functional groups along a polymer chain and the presence of bulky side groups would also significantly decrease the degree of interassociation hydrogen bonding.[62] In the present case, the tethered POSS side chains enhanced these effects, such that the OH groups of the phenolic resin could not interact with the C═O groups of the PMAPOSS blocks. Evidently, blending 20 wt % phenolic resin into the well-defined hexagonally packed PMMA cylindrical structure ($PMMA_{123}$-*b*-$PMAPOSS_{41}$) increased the degree of interassociation hydrogen bonding between the C═O groups of the PMMA block and OH groups of the phenolic resin, relative to that in the well-defined PMMA lamellar structure ($PMMA_{189}$-*b*-$PMAPOSS_{34}$). In a two-dimensional-confined PMMA cylindrical structure, the possibility of a polymer chain bending back on itself is lower, and the steric crowding and shielding effects are less significant; thus, the fraction of interassociation hydrogen bonds is enhanced. Upon increasing the phenolic content to 40 wt % in the three PMMA-*b*-PMAPOSS block copolymers, the lamellar structure of $PMMA_{189}$-*b*-$PMAPOSS_{34}$ changed to the short-range order of a hexagonally packed PMAPOSS cylindrical structure, whereas the relatively higher volume fractions of PMAPOSS caused the $PMMA_{119}$-*b*-$PMAPOSS_{26}$ and $PMMA_{123}$-*b*-$PMAPOSS_{41}$ blends to retain their lamellar structures. At this phenolic content, increasing the PMAPOSS weight fraction in the block copolymer decreased the fraction of intermolecular hydrogen bonding, although the values remained higher than those in phenolic/PMMA blends. With further increase of the phenolic content to 60 wt %, all blends exhibited the short-range order of cylindrical or lamellar structures, as shown in Figures 8d, 8i, and 8n. At relatively low weight fractions of PMAPOSS in the $PMMA_{189}$-*b*-$PMAPOSS_{34}$ block copolymer, the fraction of hydrogen-bonded C═O groups remained higher than those in phenolic/PMMA blends, implying that the OH groups of the phenolic resin could still interact with the C═O groups of the PMMA block segment, thereby allowing the morphological change to occur in this case. In contrast, the increased weight fractions of the PMAPOSS blocks in the $PMMA_{119}$-*b*-$PMAPOSS_{26}$ and $PMMA_{123}$-*b*-$PMAPOSS_{41}$ block copolymers caused the fractions of intermolecular hydrogen bonds to be lower than those in phenolic/PMMA blends, implying that the OH groups of the phenolic resin had difficulty interacting with the C═O groups of the PMMA block segments; accordingly, the lamellar structure changed from highly ordered to that with short-range order. Further increase of the phenolic content to 80 wt % caused all blends to exhibit disorder or macrophase separation, as revealed in Figures 9e, 9j, and 9o. Evidently, all phenolic/PMMA-*b*-PMAPOSS blends featured relatively lower fractions of hydrogen-bonded C═O groups in the PMMA blocks compared with phenolic/PMMA blends. The PMAPOSS block segments were dispersed in a continuous phenolic/

dx.doi.org/10.1021/ma502180c | *Macromolecules* 2014, 47, 8709−8721

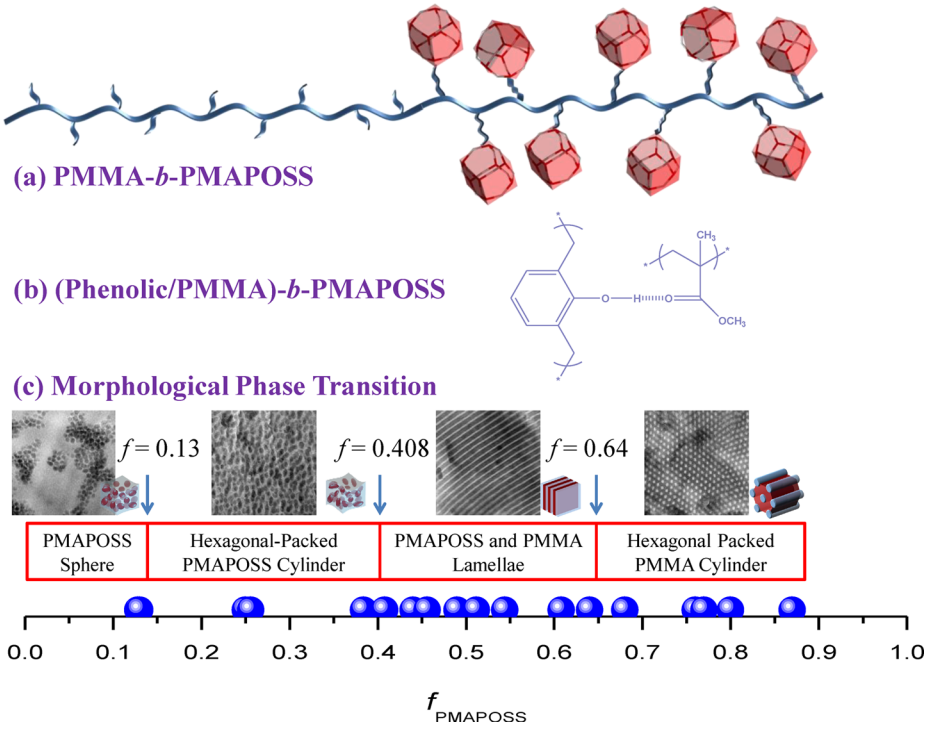

Figure 10. Schematic representations of (a) PMMA-*b*-PMAPOSS, (b) hydrogen bond between the OH groups of the phenolic resin and C═O groups of the PMMA block, and (c) morphological phase transitions of PMMA-*b*-PMAPOSS after blending with the phenolic resin.

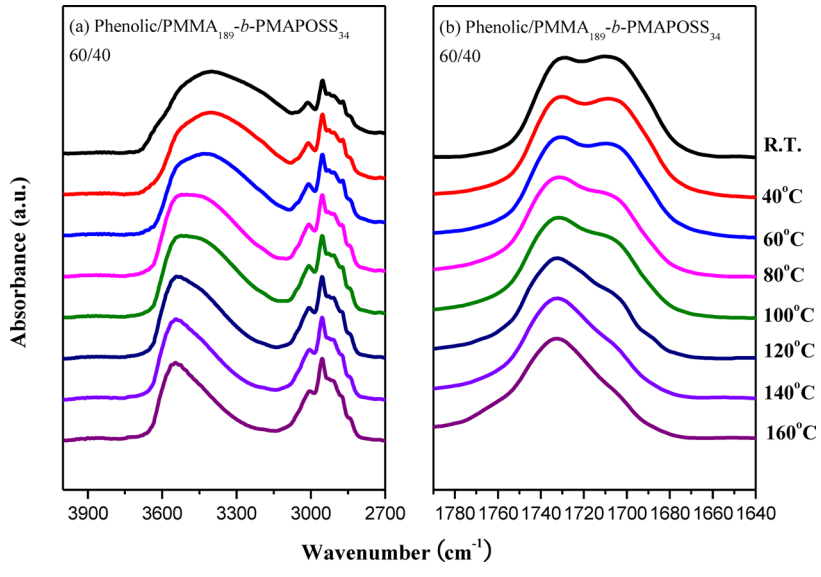

Figure 11. FTIR spectra of phenolic/$PMMA_{189}$-*b*-$PMAPOSS_{34}$ (60/40) recorded at various temperatures: (a) OH and (b) C═O stretching.

PMMA matrix at 80 wt % phenolic content. For the block copolymer having the highest PMAPOSS weight fraction ($PMMA_{123}$-*b*-$PMAPOSS_{41}$), the fraction of intermolecular hydrogen bonds did not increase upon increasing the phenolic content, implying that the tethered POSS side chains actually enhanced the screening effect of the phenolic/PMMA miscible phase and led to macrophase separation. Figure 10 summarizes the well-defined microphase-separated structures of all PMMA-*b*-PMAPOSS copolymers at various volume fractions of PMAPOSS and their blends with the phenolic resin, in addition to those of pure PMMA-*b*-PMAPOSS diblock copolymers studied previously.[35] Upon increasing the PMAPOSS volume fraction, PMAPOSS spheres, the short-range order of hexagonally packed PMAPOSS cylinders, PMAPOSS lamellae, and hexagonally packed PMMA cylinders were observed. Because a copolymer containing a relatively higher volume fraction of PMAPOSS was difficult to prepare, PMMA spheres were not observed in this study. Most importantly, an order−order transition mediated by hydrogen-bonding interactions could be induced by simply blending the phenolic resin into PMMA-*b*-PMAPOSS block copolymers.

Self-Assembly of Phenolic/PMMA-*b*-PMAPOSS Blends at Various Temperatures. It was also interesting to examine the behavior of phenolic/PMMA-*b*-PMAPOSS blends with variation in temperature. Figure 11 presents the FTIR spectra of the phenolic/$PMMA_{189}$-*b*-$PMAPOSS_{34}$ (60/40) blend

dx.doi.org/10.1021/ma502180c | *Macromolecules* 2014, 47, 8709−8721

measured at temperatures ranging from 25 to 160 °C. The intensity of the signal for the free OH groups increased gradually, and the signal for the hydrogen-bonded OH and C═O groups shifted to higher wavenumbers upon increasing the temperature, indicating the dissociation of hydrogen bonds in this blend, as expected (Figure 11a). In addition, the fraction of hydrogen-bonded C═O groups in the PMMA segment decreased upon increasing the temperature (Figure 11b), as is usually the case.[51−53] Figure 12 displays the SAXS profiles of

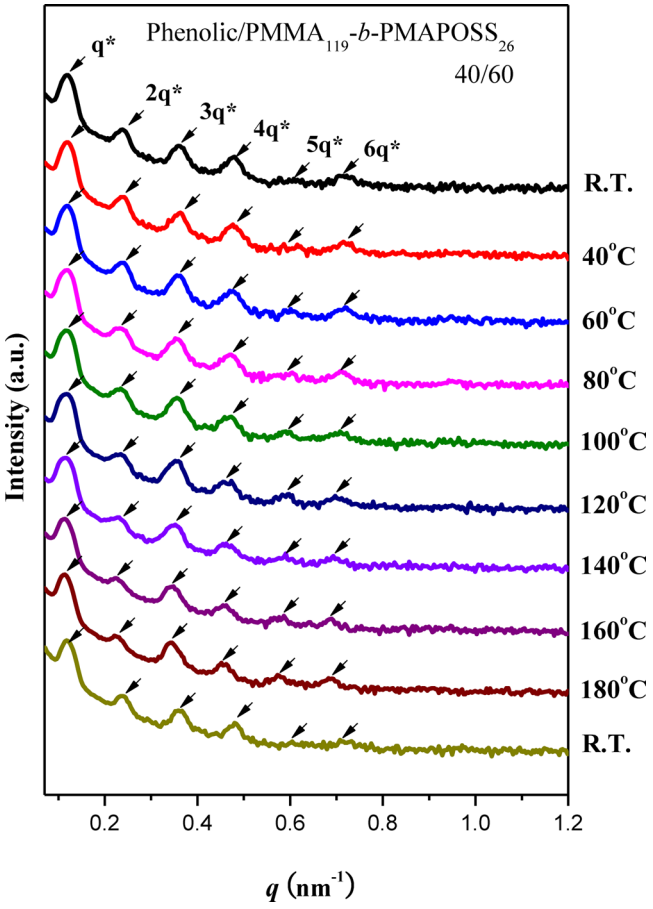

Figure 12. SAXS patterns of phenolic/$PMMA_{119}$-*b*-$PMAPOSS_{26}$ (40/60) at various temperatures.

the phenolic/$PMMA_{189}$-*b*-$PMAPOSS_{34}$ (40/60) blend recorded at various temperatures. The high order ratios of the patterns did not change upon increasing the temperature, indicating that this blend also possessed a lamellar structure. Only the first-order scattering position shifted slightly to the lower q region upon increasing the temperature; however, it exhibited reversible behavior when the sample was cooled to room temperature. Although the degree of interassociation hydrogen bonding decreased upon increasing the temperature, the lamellar structure was maintained, indicating that the phenolic resin was still in the PMMA domain and did not change its self-assembled structure. This phenomenon usually occurs in block copolymer/homopolymer blends;[64,65] the phenolic resin preferentially resides in the PMMA domain, rather than the PMAPOSS domain, presumably because the solubility parameter of the phenolic resin is closer to PMMA than to PMAPOSS.

WAXD Analyses of Phenolic/PMMA-*b*-PMAPOSS Blends. Figure 13a presents the X-ray diffraction patterns of

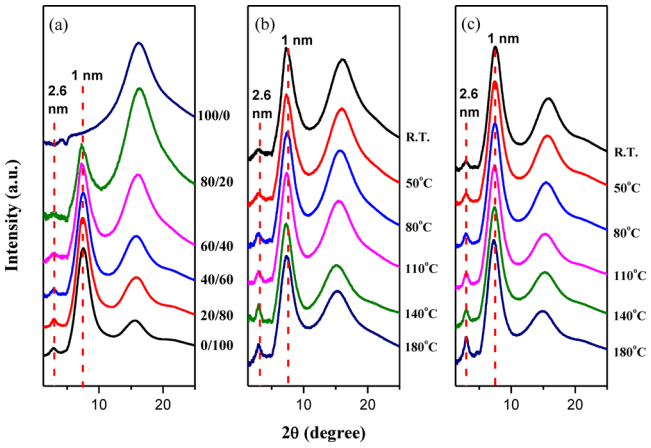

Figure 13. WAXD patterns of (a) phenolic/$PMMA_{119}$-*b*-$PMAPOSS_{26}$ blends at various phenolic compositions recorded at room temperature and (b) phenolic/$PMMA_{119}$-*b*-$PMAPOSS_{26}$ (60/40) and (c) phenolic/$PMMA_{119}$-*b*-$PMAPOSS_{26}$ (40/60) recorded at various temperatures.

the phenolic/$PMMA_{119}$-*b*-$PMAPOSS_{26}$ blends at room temperature. Pure PMAPOSS had two major diffraction peaks at 2θ = 7.50° and 15.99°, corresponding to *d*-spacings of 1.0 and 0.49 nm, respectively.[35,66] The first is consistent with the size of a POSS unit and arose from its rhombohedral crystal structure,[67] where the *d*-spacing of 0.49 nm is the average distance between the $COOCH_2$ groups of the PMMA or PMAPOSS segments, as revealed in Scheme 3a.[35] No X-ray diffraction peaks were

Scheme 3. Schematic Representation of (a) Relevant Length Scale in PMAPOSS and (b) Possible Phase Structure of the Phenolic/PMMA-*b*-PMA Blend, Where (c) PMAPOSS Assumes a Helixlike Structure

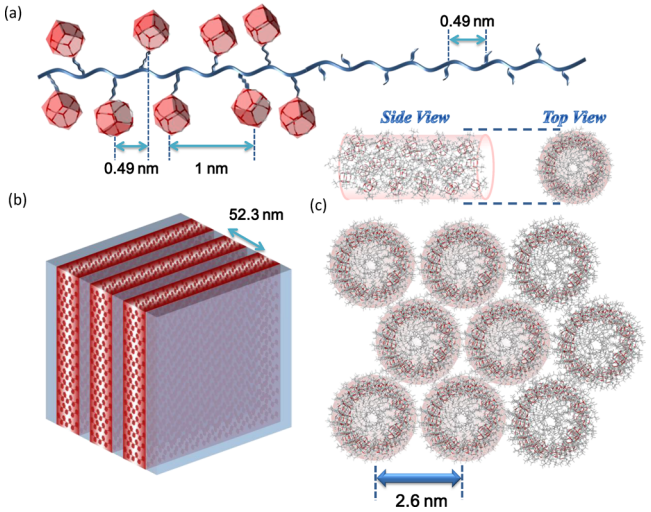

discernible for the pure phenolic resin; only an amorphous halo appeared at 2θ = 16.23° in Figure 13a. A weak diffraction peak at 2θ = 3.0° was also observed, corresponding to a *d*-spacing of 2.6 nm, in the X-ray diffraction patterns of the PMAPOSS segment and phenolic/$PMMA_{119}$-*b*-$PMAPOSS_{26}$ blends, presumably representing the average distance between the main

dx.doi.org/10.1021/ma502180c | Macromolecules 2014, 47, 8709−8721

chains of PMAPOSS.[35] Jin et al.[35] reported that PMAPOSS chains are randomly oriented without any short- or long-range order in solvent-annealed films, whereas in thermally annealed films, the chains form regularly packed molecular cylinders in a helical conformation in the orthorhombic lattice unit cell as a result of the crystallization of POSS moieties. Through simulation, it was estimated that the spacing of the PMAPOSS chains in the helical conformation is approximately 2.5 nm.[35] The WAXD patterns of phenolic/$PMMA_{119}$-*b*-$PMAPOSS_{26}$ (60/40 and 40/60 in Figures 13b and 13c, respectively) at various temperatures were also investigated. The intensity of the diffraction peak at $2\theta = 3.0°$ increased upon increasing the temperature, indicating that thermal annealing of the PMAPOSS main chains indeed enhanced the regular packing of molecular cylinders in a helical conformation in the orthorhombic lattice unit cell.[35] Scheme 3 illustrates the hierarchical self-assembled structure of phenolic/$PMMA_{119}$-*b*-$PMAPOSS_{26}$ (40/60) and relevant length scale in PMMA-*b*-PMAPOSS, where PMAPOSS assumed a helixlike structure. Hierarchical self-assembled structures were observed in these phenolic/$PMMA_{119}$-*b*-$PMAPOSS_{26}$ blends, including the microphase-separation-induced self-assembly of a lamellar structure between the phenolic/PMMA and PMAPOSS domains (d = 52.3 nm, Scheme 3b) and POSS-aggregation-driven packing into a hexagonal lattice oriented perpendicular to the direction of the lamellar structure where the spacing of the PMAPOSS chains in the helical conformation was approximately 2.6 nm (Scheme 3c).

CONCLUSION

We prepared a series of PMMA-*b*-PMAPOSS block copolymers through anionic polymerization and investigated the properties of their blends with a phenolic resin using DSC, FTIR, SAXS, TEM, and WAXD analyses. The OH groups of the phenolic resin only formed intermolecular hydrogen bond interactions with the C═O groups of the PMMA segments; such interactions did not occur with those of the PMAPOSS segments owing to a strong screening effect induced by the tethered POSS side chains. TEM and SAXS analyses indicated that the phenolic/PMMA-*b*-PMAPOSS blends underwent a series of phase transitions mediated by hydrogen bond interactions upon increasing the phenolic content, depending on the weight fraction of the PMAPOSS segment in the block copolymer. Hierarchical self-assembled structures—hexagonally packed cylindrical or lamellar nanostructures—formed from the block copolymer segments, with POSS aggregates packed into hexagonal lattices oriented perpendicular to the direction of the nanostructures.

AUTHOR INFORMATION

Corresponding Authors

*E-mail kuosw@faculty.nsysu.edu.tw; Tel 886-7-5252000 ext 4079; Fax 886-7-5254099 (S.-W.K.).

*E-mail hayakawa.t.ac@m.titech.ac.jp (T.H.).

Notes

The authors declare no competing financial interest.

ACKNOWLEDGMENTS

This study was supported financially by the National Science Council, Taiwan, Republic of China, under Contracts MOST103-2221-E-110-079-MY3 and MOST102-2221-E-110-008-MY3. Mr. Lin thanks the 2012 Summer Program of the Interchange Association of Japan that helped initiate this study. We also thank Mr. Hsien-Tsan Lin of the Regional Instruments Center at National Sun Yat-Sen University for his assistance with the TEM experiments.

REFERENCES

(1) Rodriguez-Hernandez, J.; Chécot, F.; Gnanou, Y.; Lecommandoux, S. *Prog. Polym. Sci.* **2005**, *30*, 691−724.

(2) Förster, S.; Antonietti, M. *Adv. Mater.* **1998**, *10*, 195−217.

(3) Chen, S. C.; Kuo, S. W.; Chang, F. C. *Langmuir* **2011**, *27*, 10197−10205.

(4) Shen, H. W.; Zhang, L. F.; Eisenberg, A. *J. Am. Chem. Soc.* **1999**, *121*, 2728−2740.

(5) Ruokolainen, J.; Saariaho, M.; Ikkala, O.; ten Brinke, G.; Thomas, E. L.; Torkkeli, M.; Serimaa, R. *Macromolecules* **1999**, *32*, 1152−1158.

(6) Chu, W. C.; Li, J. G.; Wang, C. F.; Jeong, K. U.; Kuo, S. W. *J. Polym. Res.* **2013**, *20*, 272.

(7) Park, I.; Park, S.; Park, H. W.; Chang, T.; Yang, H.; Ryu, C. Y. *Macromolecules* **2006**, *39*, 315−318.

(8) Tsai, H.; Pitera, J. W.; Miyazoe, H.; Bangsaruntip, S.; Engelmann, S. U.; Liu, C. C.; Cheng, J. Y.; Bucchignano, J. J.; Klaus, D. P.; Joseph, E. A.; Sanders, D. P.; Colburn, M. E.; Guillorn, M. A. *ACS Nano* **2014**, *8*, 5227−5232.

(9) Kuo, S. W.; Tung, P. H.; Lai, C. L.; Jeong, K. U.; Chang, F. C. *Macromol. Rapid Commun.* **2008**, *29*, 229−233.

(10) Chen, S. C.; Kuo, S. W.; Jeng, U. S.; Chang, F. C. *Macromolecules* **2010**, *43*, 1083−1092.

(11) Lu, C. H.; Chang, F. C.; Kuo, S. W. *Macromol. Chem. Phys.* **2010**, *211*, 1339−1347.

(12) Park, S. C.; Kim, B. J.; Hawker, C. J.; Kramer, E. J.; Bang, J.; Ha, J. S. *Macromolecules* **2007**, *40*, 8119−8124.

(13) Kim, B. J.; Fredrickson, G. H.; Kramer, E. J. *Macromolecules* **2008**, *41*, 436−447.

(14) Yeh, S. W.; Wei, K. H.; Sun, Y. S.; Jeng, U. S.; Liang, K. S. *Macromolecules* **2005**, *38*, 6559−6565.

(15) Lu, C. H.; Kuo, S. W.; Chang, W. T.; Chang, F. C. *Macromol. Rapid Commun.* **2009**, *30*, 2121−2127.

(16) Kuo, S. W.; Yang, H. Y. *Macromol. Chem. Phys.* **2011**, *212*, 2249−2259.

(17) Jang, S. G.; Kramer, E. J.; Hawker, C. J. *J. Am. Chem. Soc.* **2011**, *133*, 16986−16996.

(18) Lin, Y.; Daga, V. K.; Anderson, E. R.; Gido, S. P.; Watkins, J. J. *J. Am. Chem. Soc.* **2011**, *133*, 6513−6516.

(19) Daga, V. K.; Anderson, E. R.; Gido, S. P.; Watkins, J. J. *Macromolecules* **2011**, *44*, 6793−6799.

(20) Noro, A.; Higuchi, K.; Sageshima, Y.; Matsushita, Y. *Macromolecules* **2012**, *45*, 8013−8020.

(21) Jang, S. G.; Khan, A.; Hawker, C. J.; Kramer, E. J. *Macromolecules* **2012**, *45*, 1553−1561.

(22) Lin, T.; Ho, R. M.; Ho, J. C. *Macromolecules* **2009**, *42*, 742−751.

(23) Ramna, V.; Sharma, R.; Hatton, T. A.; Olsen, B. D. *ACS Macro Lett.* **2013**, *2*, 655−659.

(24) Son, J. G.; Hannon, A. F.; Gotrik, K. W.; Alexander-Katz, A.; Ross, C. A. *Adv. Mater.* **2011**, *23*, 634−639.

(25) Borah, D.; Ozmen, M.; Rasappa, S.; Shaw, M. T.; Holmes, J. D.; Morris, M. A. *Langmuir* **2013**, *29*, 2809−2820.

(26) Nunns, A.; Gwyther, J.; Manners, I. *Polymer* **2013**, *54*, 1269−1284.

(27) Wu, Y. C.; Kuo, S. W. *J. Mater. Chem.* **2012**, *22*, 2982−2991.

(28) Kuo, S. W.; Chang, F. C. *Prog. Polym. Sci.* **2011**, *36*, 1649−1696.

(29) Yu, X.; Yue, K.; Hsieh, I. F.; Li, Y.; Dong, X. H.; Xin, Y.; Wang, H. F.; Shi, A. C.; Newkome, G. R.; Ho, R. M.; Chen, E. Q.; Zhang, W. B.; Cheng, S. Z. D. *Proc. Natl. Acad. Sci. U. S. A.* **2013**, *110*, 10078−10083.

(30) Zhang, W. B.; Yu, X.; Wang, C. L.; Sun, H. J.; Hsieh, I. F.; Li, Y.; Dong, X. H.; Yue, K.; Horn, R. V.; Cheng, S. Z. D. *Macromolecules* **2014**, *47*, 1221−1239.

(31) Pyun, J.; Matyjaszewski, K. *Macromolecules* **2000**, *33*, 217−220.

(32) Pyun, J.; Matyjaszewski, K.; Wu, J.; Kim, G. M.; Chun, S. B.; Mather, P. T. *Polymer* **2003**, *44*, 2739−2750.
(33) (a) Xu, Y. T.; Chen, M.; Xie, J.; Li, C.; Yang, C. J.; Deng, Y. M.; Yuan, C. H.; Chang, F. C.; Dai, L. Z. *React. Funct. Polym.* **2013**, *73*, 1646−1655. (b) Deng, Y.; Bernard, J.; Alcouffe, P.; Galy, J.; Dai, L.; Gerard, J. F. *J. Polym. Sci., Part A: Polym. Chem.* **2011**, *49*, 4343−4352. (c) Wang, L.; Li, J.; Li, L.; Zheng, S. *J. Polym. Sci., Part A: Polym. Chem.* **2013**, *51*, 2079−2090.
(34) Lin, Y. C.; Kuo, S. W. *Polym. Chem.* **2012**, *3*, 882−891.
(35) Hirai, T.; Leolukman, M.; Jin, S.; Goseki, R.; Ishida, Y.; Kakimoto, M.; Hayakawa, T.; Ree, M.; Gopalan, P. *Macromolecules* **2009**, *42*, 8835−8843.
(36) Kuo, S. W. *Polym. Int.* **2009**, *58*, 455−464.
(37) Lee, H. F.; Kuo, S. W.; Huang, C. F.; Lu, J. S.; Chan, S. C.; Wang, C. F.; Chang, F. C. *Macromolecules* **2006**, *39*, 5458−5465.
(38) Matsushita, Y. *Macromolecules* **2007**, *40*, 771−776.
(39) Hameed, N.; Guo, Q. *Macromolecules* **2008**, *41*, 7596−7605.
(40) Dobrosielska, K.; Wakao, S.; Takano, A.; Matsushita, Y. *Macromolecules* **2008**, *41*, 7695−7698.
(41) Dobrosielska, K.; Wakao, S.; Suzuki, J.; Noda, K.; Takano, A.; Matsushita, Y. *Macromolecules* **2009**, *42*, 7098−7102.
(42) Chen, W. C.; Kuo, S. W.; Jeng, U. S.; Chang, F. C. *Macromolecules* **2008**, *41*, 1401−1410.
(43) Chen, W. C.; Kuo, S. W.; Lu, C. H.; Chang, F. C. *Macromolecules* **2009**, *42*, 3580−3590.
(44) Lin, I. H.; Kuo, S. W.; Chang, F. C. *Polymer* **2009**, *50*, 5276−5287.
(45) Li, J. G.; Lin, Y. D.; Kuo, S. W. *Macromolecules* **2011**, *44*, 9295−9309.
(46) Huang, C. F.; Kuo, S. W.; Lin, H. C.; Chen, J. K.; Chen, Y. K.; Xu, H. Y.; Chang, F. C. *Polymer* **2004**, *45*, 5913−5921.
(47) Huang, C. F.; Kuo, S. W.; Lin, F. L.; Huang, W. J.; Wang, C. F.; Chen, W. Y.; Chang, F. C. *Macromolecules* **2006**, *39*, 300−308.
(48) Chiou, C. W.; Lin, Y. C.; Wang, L.; Hirano, C.; Suzuki, Y.; Hayakawa, T.; Kuo, S. W. *Polymers* **2014**, *6*, 926−948.
(49) Lin, H. C.; Kuo, S. W.; Huang, C. F.; Chang, F. C. *Macromol. Rapid Commun.* **2006**, *27*, 537−541.
(50) Kwei, T. K. *J. Polym. Sci., Polym. Lett. Ed.* **1984**, *22*, 307−313.
(51) Coleman, M. M.; Painter, P. C. *Prog. Polym. Sci.* **1995**, *20*, 1−59.
(52) He, Y.; Zhu, B.; Inoue, Y. *Prog. Polym. Sci.* **2004**, *29*, 1021−1051.
(53) Kuo, S. W. *J. Polym. Res.* **2008**, *15*, 459−486.
(54) Kuo, S. W.; Tung, P. H.; Chang, F. C. *Macromolecules* **2006**, *39*, 9388−9395.
(55) Roe, R. J. *Methods of X-ray and Neutron Scattering in Polymer Science*; Oxford University Press: New York, 2000.
(56) Hashimoto, T.; Koizumi, S.; Hasegawa, H.; Izumitani, T.; Hyde, S. T. *Macromolecules* **1992**, *25*, 1433−1439.
(57) Koizumi, S.; Hasegawa, H.; Hashimoto, T. *Macromolecules* **1994**, *27*, 6532−6540.
(58) Coleman, M. M.; Xu, Y.; Painter, P. C. *Macromolecules* **1994**, *27*, 127−134.
(59) Painter, P. C.; Veytsman, B.; Kumar, S.; Shenoy, S.; Graf, J. F.; Xu, Y.; Coleman, M. M. *Macromolecules* **1997**, *30*, 932−942.
(60) Coleman, M. M.; Pehlert, G. J.; Painter, P. C. *Macromolecules* **1996**, *29*, 6820−6831.
(61) Pehlert, G. J.; Painter, P. C.; Veytsman, B.; Coleman, M. M. *Macromolecules* **1997**, *30*, 3671−3677.
(62) Pehlert, G. J.; Painter, P. C.; Coleman, M. M. *Macromolecules* **1998**, *31*, 8423−8424.
(63) Coleman, M. M.; Guigley, K. S.; Painter, P. C. *Macromol. Chem. Phys.* **1999**, *200*, 1167−1173.
(64) Ho, R. M.; Chiang, Y. W.; Lin, C. C.; Huang, B. H. *Macromolecules* **2005**, *38*, 4769−4779.
(65) Ho, R. M.; Chiang, Y. W.; Lin, C. C.; Bai, S. J. *Macromolecules* **2002**, *35*, 1299−1306.
(66) Jin, S.; Hira, T.; Ahn, B.; Rho, Y.; Kim, K. W.; Kakimoto, M. A.; Gopalan, P.; Hayakawa, T.; Ree, M. *J. Phys. Chem. B* **2010**, *114*, 8033−8042.
(67) Chen, Y.; Kang, E. T. *Mater. Lett.* **2004**, *58*, 3716−3719.